Designing Optical Systems for Terahertz Spectroscopy

A Major Qualifying Project Report:

Submitted to the faculty of

WORCESTER POLYTECHNIC INSTITUTE

In partial fulfillment of the Requirements for the Degree of Bachelor of Science

Date: 6 May 2021

Submitted By:

Jaden Chin

Approved By:

Dr. Douglas Petkie

Acknowledgements

This project would not have been possible without the help of Dr. Doug Petkie and Jacob Bouchard. Dr. Petkie served as the primary advisor for the project and helped define its scope throughout its development. Jacob is a PhD student at WPI with extensive experience in THz spectroscopy who served as an additional advisor to this project. The Gateway Lab Manager, James Eakin, also made vital contributions to the maintenance and functionality of the lab equipment used in this project. I would like to thank each of these contributors as well as WPI for the opportunity to complete this as my capstone project.

Abstract

Terahertz Imaging is an emerging technology with applications in medical imaging, non-destructive evaluation, and wireless communication. Recent developments in efficient THz wave production allows for new studies to be conducted to observe the behaviors of materials in the THz wave spectrum. The objective of this paper is to develop method for characterizing these materials, and addresses sources of error that arise in THz optical systems. This was achieved through the use of the Toptica TeraFlash, a pulsed THz wave generator, and an accompanying imaging gantry. Effective methods were identified for calculating the refractive index and absorption coefficient of materials in the THz spectrum. Additionally, focal displacement was found to be a source of unavoidable error given the current imaging gantry. A new imaging platform was then designed that allows for vertical translation of the TeraFlash receiver. This will allow for a scan of the Gaussian Beam produced by the TeraFlash in order to identify a configuration that will minimize the effects focal displacement on collected data.

Table of Contents

List of Figures

List of Tables

Introduction

The rapid development of wireless communication can be largely attributed to the need for increased bandwidth and improved utilization of the mm wavelength spectrum. These frequencies allowed for the development of 5G communication that boasts data rates of 0.1-0.5 Gbps. This rate is serviceable for basic communication, but this frequency spectrum may be vastly improved upon by the use of terahertz waves. The terahertz electromagnetic spectrum consists of frequencies ranging from 0.1 THz to 10 THz and is one of the least researched frequency bands in the electromagnetic spectrum. If this spectrum is used properly, it has the potential to boast a latency of 0.1 ms, data rates of 10 Gbps, and a peak data rate of 1 Tbit/s (Chong, 2019). These advancements could lead to the implementation of terahertz based technologies such as micro-cells, THz WIFI, databases and satellites.

While certain aspects have detailed studies, some areas need additional research into the propagation of THz waves through free space, and how these waves are impacted by atmospheric conditions and ground clutter. It is theorized that aerosol and water vapor are the main granules that contribute to THz attenuation in the atmosphere. A depiction of the absorption spectrum of THz waves in Figure 1.
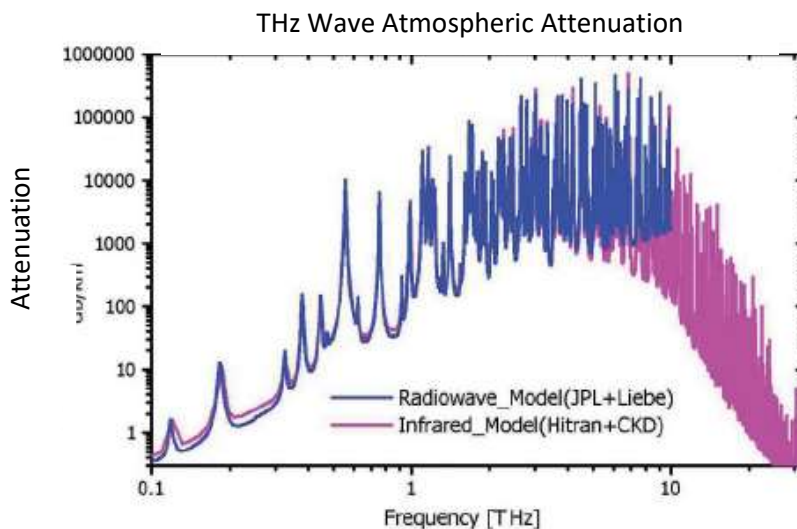
Figure 1. A measure of the absorption of THz waves through the atmosphere with respect to frequency.

As you can see in Figure 1, the absorption of THz waves in the atmosphere follows a general curve with a peak at approximately 5 THz. Along this curve, there are dramatic spikes in absorption as well as pockets of high propagation. Therefore, when designing communication systems, it is important to use frequencies that fall into these pockets of low absorption. Absorption of electromagnetic waves tends to increase with frequency due to higher energy waves interacting with more atoms throughout its propagation. THz waves bridge the gap between wavelengths that pass through most materials at microwave frequencies, and wavelengths that do not in the infrared region.

While more research into THz propagation is required, so is research about how THz waves interact with materials used to construct optical components. These components include lenses, sources, and receivers and are used not only in research but in commercial products as well. Receivers are the most well researched out of the three, and at this time they are developed enough to detect THz waves over short and long distances. THz sources are more difficult to develop than receivers due to limitations on traditional designs. Most sources are based on semiconductors which experience high resistive loss and high frequency roll off in the THz range. However, recent designs that use frequency conversion to alter mm wavelengths have found consistent success. The development of lenses relies largely on accurate measurements of THz properties of different materials (Karpowicz, 2005). This requires the development of reliable receivers and sources and is therefore the last to be studied out of the three components. By designing optical systems that can accurately measure optical properties of materials in the THz range, we may accelerate the progress towards 6G communication.

Background

Measuring Optical Properties

The design of any optical technology requires accurate knowledge about the optical properties of the materials used. Two of the standard measurements used when characterizing materials are their refractive index and absorption coefficient. The refractive index is a dimensionless measure of the speed of light through a specified medium. When light waves pass through an object with a different refractive index, it is slowed and refracted at an angle dependent on the incident angle of the beam and the ratio of the two refractive indices. This angle of refraction may be calculated using Snell's law and can be used to predict the path of propagated light through materials. The basic equation for the refractive index may be found below in Eq. 1 where c is the speed of light, v is the wave's speed in the material, and n is the refractive index.

$$v = \frac{c}{n} \tag{1}$$

The absorption coefficient indicates how deep light can penetrate a material and is often measured in cm^{-1}. The value of the absorption coefficient may be determined using the Beer Lambert law. This law considers the molecular concentration of the material, as well as its absorptivity. The equation that corresponds to this law may be found below in Eq. 2 where A is absorbance, ε is the molar absorptivity, b is the length of the light path, and C is the concentration. The absorption coefficient may also be calculated using the proportion of power transmitted through a material while taking its thickness and refractive index into consideration. These two factors are the basic characteristics used when selecting materials to design optical systems.

$$A = \varepsilon b C \tag{2}$$

To measure these characteristics, optical systems will often make use of spectroscopy through the use of reflection or transmission. Reflection spectroscopy consists of using a transmitter to propagate radiation through space where it interacts with a physical material. Depending on the optical properties of the material, a portion of the incident energy will be absorbed and transmitted by the material, and a portion will be reflected. The reflected portion is then captured by a receiver and converted to a digital output. Transmission follows a similar process, except instead of recording energy reflected off the material, the receiver is placed on the other side of the sample. In doing so, it captures the amount of energy that passes through the sample. The primary measurements from both forms of spectroscopy are the power either reflected or transmitted through the sample, and the phase difference of the THz wave between the transmitter and receiver. Alone, this data is not significant, but when it is compared to a reference signal in which the THz wave is propagated through air, the fraction of absorbed power can be calculated. The index of refraction can then be calculated using the equation shown below.

$$n(f) = 1 + \frac{\varphi(f)c}{2\pi f d} \tag{3}$$

Where $\varphi(f)$ is the phase shift, c is the speed of light, f is the frequency of the wave being propagated, and d is the thickness of the sample. This equation translates the difference in phase to a physical distance and divides that distance by the thickness of the sample. Then, by adding this difference to the refractive index of our reference ($n_{air} \approx 1$) to get the refractive index of the material. This data processing strategy is shown to accurately calculate the index of refraction in the THz domain (Zhang, 2018).

The absorption coefficient may then be calculated using the index of refraction, and the fractional power received when the sample is in place. The equation below shows how to calculate the absorption coefficient using the fractional power received, the index of refraction, and the thickness of the sample. In Eq. 4, α is the absorption coefficient, d is the thickness of the sample, $A(f)_{Ref}$ is the amplitude of the reference signal, $A(f)_{Sam}$ is the amplitude of the sample signal, and $n(f)$ is the refractive index at a given frequency.

$$\alpha(f) = \left(\frac{2}{d}\right) \ln\left\{\left[\frac{A(f)_{ref}}{A(f)_{samp}}\right]\left[\frac{4n(f)}{(n(f)+1)^2}\right]\right\} \tag{4}$$

Calculation of both the absorption coefficient and refractive index are based on differences in power and phase between reference and sample measurements. These equations have yielded results consistent with literature measurements of the same materials in the THz spectrum. The system used to verify these equations was a time domain transmission system, but these equations can also be used with data from a reflection system. Using these equations, we may collect data about the optical properties of different materials in the THz wave spectrum. As an emerging field in optics, there is little research done on the properties of different materials, but these methods can be verified by replicating studies that have produced well accepted conclusions.

Optical THz systems produce data for these calculations by measuring the amplitude of the electric field of the wave. This is generally done by producing a charge carrying wave with an emitter that propagates through a sample to a receiver. These charge carriers interact with the sample and may be absorbed, reflected, or slowed down. When the wave interacts with the receiver, the electromagnetic field then generates a photocurrent that is directly proportional to the THz electric field (Toptica, 2021). This current may be measured as an electric field as a function of time and may then be converted to frequency domain analysis using a fast Fourier transform.

Optical Systems

For the purpose of designing and using optical systems, Gaussian beam optics are used to model the propagation of light. A Gaussian beam is simply a beam of light whose intensity is radially symmetric and whose distribution is described by a Gaussian function. This type of beam assumes small divergence angles and allows beam physics to be simplified with minimal error in most practical uses. Figure 2 shows a graphical representation of the intensity of a Gaussian beam with respect to the radial distance from the axial center of propagation.
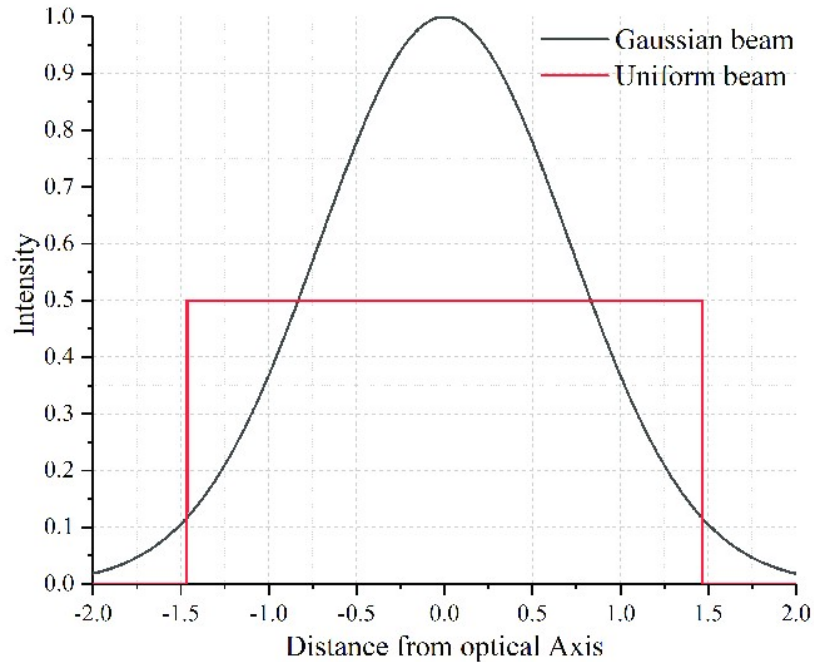
Figure 2. Graph of the relationship between and intensity and axial radius of a Gaussian and uniform beam. The graph is unitless and serves to represent general behaviors of these two models.

It should be noted that this is modeled after the fundamental Hermite Gaussian mode. Any electric field pattern produced by radiation should be able to be explained by orthogonal gaussian functions. Combinations of these different functions create unique intensity profiles that can change throughout the beam's propagation. Different intensity profiles change the way radiation needs to be captured, and the more complex the function is, the more difficult it is to build an antenna that maximizes the signal received. Fortunately, well designed transmitters limit the effects of higher order gaussians during beam propagation. Therefore, the fundamental mode is sufficient for modeling most optical systems. The Figure 3. serves as a visual representation of low order Gaussian modes, with the fundamental mode in Figure 2. given by the TEM_{00} mode in Figure 3.
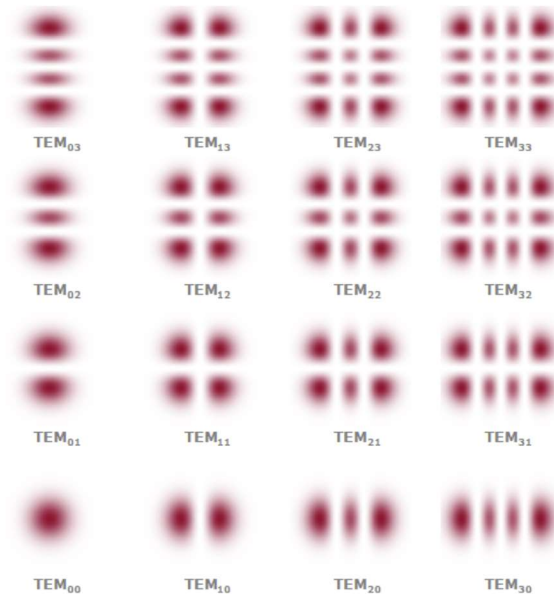
Figure 3. Intensity profiles of low order Gaussian modes. Note that the left subscript indicates higher order modes on the horizontal axis and the right subscript indicates mode on the vertical axis.

In a Gaussian beam, the axial radius approaches infinity as the intensity approaches zero. This model therefore requires a clear definition of the outer boundaries of the beam in order to evaluate beam characteristics such as divergence. The first definition of the beam boundaries is the beam radius which is defined as the point in which the radial axis approaches an intensity approximately $\frac{1}{e^2}$ or 13.5% of its maximum. Using this definition, we may assume small angle divergence in order to develop other useful beam characteristics. For example, Rayleigh Length defines the axial distance a beam must travel for its radius to increase by a factor of $\sqrt{2}$. At this point the beam's area has doubled in size and its intensity has decreased across its distribution. There is a tradeoff depending on which definition of a beam is used when building an optical system. When using $\frac{1}{e^2}$ there is a large portion of power captured in the system, however, lenses are mirrors are not uniformly illuminated leading to less consistent resolution. Systems designed based on FWHM have more uniform resolution due to more uniformly lit lenses but capture significantly less power. When measuring optical properties of materials, it is common practice to use the $\frac{1}{e^2}$ definition to maximize the amount of radiation passing through the sample.

An alternative definition of beam radius arises from the definition of Full Width Half Maximum (FWHM) for Gaussian distributions. FWHM defines the boundaries of the beam at the diameter that marks 50% of the total beam intensity. FWHM is common in industrial applications as it is intuitive and relatively easy to calculate. There also exists a parameter Half Width Half Maximum (HWHM) which is simply half the definition of FWHM. Approximate conversions between these two definitions of beam diameter are relatively easy and may be performed using the simplified equation below.

$$FWHM = 1.18 * Beam\ Radius \tag{5}$$

When using gaussian beams for imaging, the beam may be either collimated or focused. Collimated beams are beams in which the majority of light rays travel in the same direction parallel to the direction of propagation. Collimated beams experience very little divergence and therefore have long Rayleigh lengths. Collimation is often used in labs for the purpose of propagating light across long distances. Due to the relatively constant beam radius, there is minimal power loss at the receiving component. In these cases, the beam diameter is much larger than the wavelength and the spatial resolution is low. In focused beams, light rays travel at varying angles to the axis of propagation but converge at some point along said axis and greatly increase the spatial resolution. In optical systems, beams are often focused due to a curved lens and converge at a distance from the lens equal to its focal distance. Visual representations of collimated and focused beams may be found in Figure 4.
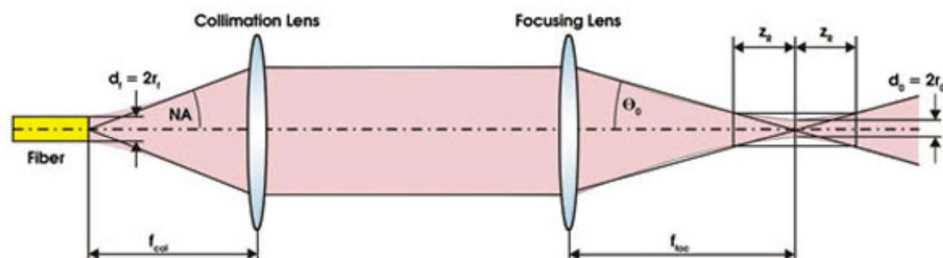
Figure 4. This figure shows the propagation of collimated light (between the two lenses) and focused light beams (to the right of the focusing lens).

Imaging can be done using either a collimated or focused beam, but for the purpose of precisely measuring optical properties, most THz systems use focused scanning. Collimated beams are advantageous due to their small divergence and wide radius. However, spatial variations of the sample will not be resolved. When using a focused beam, the sample is usually placed at the focus point so that the beam's full power may be used to image a small circular area whose radius is the beam waist. The beam waist is the minimum beam radius of focused radiation, and while most depictions of focused beams portray it as an infinitesimal point, it is a non-zero area. A perfect gaussian beam diverges equally on either side of the beam waist at a divergence angle θ.

The divergence angle is measured from the center of the beam waist between opposite edges of the beam's diameter. A perfectly collimated beam has a divergence angle of 0 degrees, but experimentally this is impossible. When designing optical systems divergence should be experimentally determined then used to achieve maximum power. Because divergence angle is measured from a point, it does not perfectly reflect the physical behavior of the beam. However, as the beam propagates further, the divergence angle more accurately reflects the beam's travel. The divergence angle may be calculated as a function of wavelength (λ) and beam waist (ω_0) as seen in Eq. 6. This phenomenon is illustrated in Figure 5.

$$\theta_{div} = \frac{\lambda}{\pi * \omega_0} \tag{6}$$
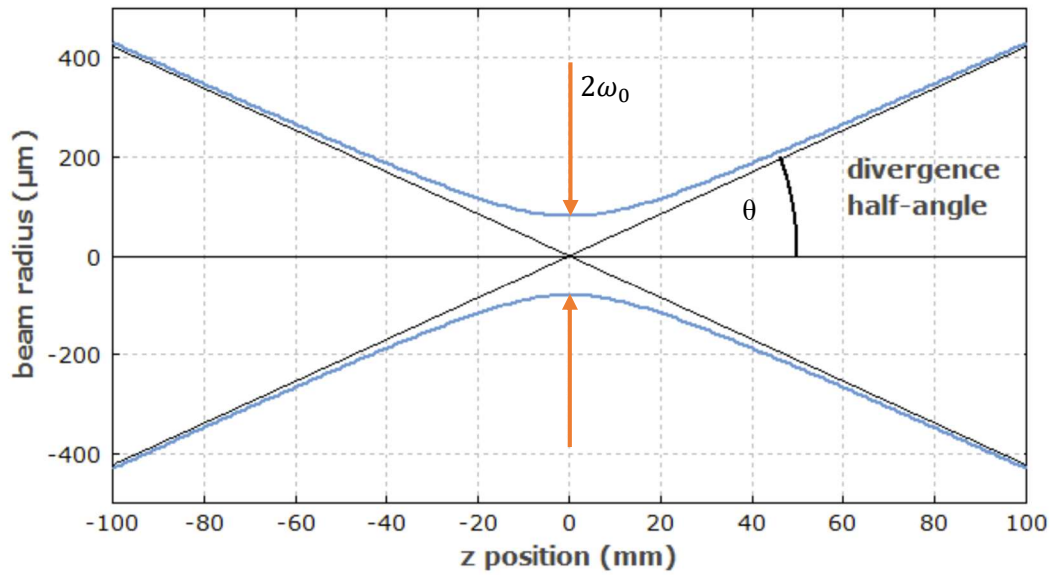
Figure 5. This figure displays the behavior of the divergence angle and how closely it approximates the behavior of the beam. As shown, the divergence angle more accurately approximates beam divergence the farther it propagates.

Focal Displacement

While focused beams are good for imaging thin samples with high spatial resolution, the Gaussian Beam becomes uncoupled when a thick sample is placed at the focal point. In imaging systems, the emitter and receiver are perfectly aligned so that the maximum amount of power in the Gaussian Beam is propagated. This alignment, however, is done with the beam propagating through air. When a thick sample is placed at the focal point of the Gaussian Beam, its refractive index causes the radiation to bend towards the normal and slightly increases the effective focal distance. This also causes the beam to have a narrower beam waist which in turn increases the divergence angle. This increased divergence angle creates an imperfect coupling between the perfectly aligned beam and the beam new beam created by the refracting sample (Liang, 2015). A diagram of this imperfect coupling may be found in Figure 6. below.
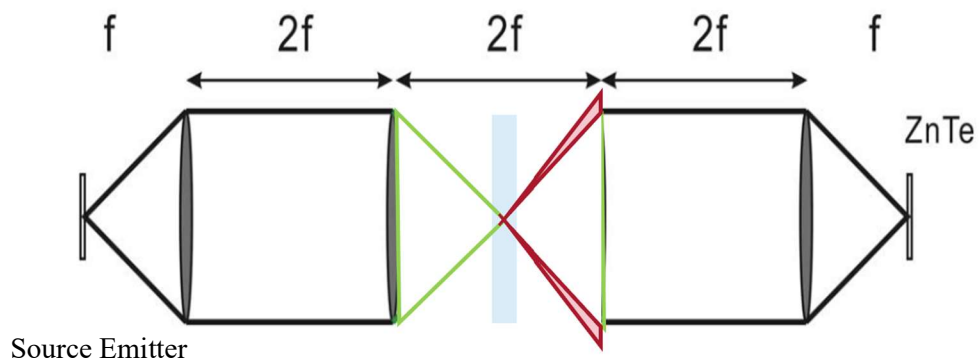
Figure 6. An imperfectly coupled Gaussian Beam with a thick sample in the middle. The green lines represent the perfectly aligned beam, and the red areas represent the power loss due to an increased divergence angle.

In this figure, the shape on the left represents the emitter, and the shape on the right represents the receiver. Because the beam is now improperly coupled, there is a power loss associated with its geometry even if there is no absorption in the sample. An increase in sample thickness corresponds to an increase in power loss, as a thicker sample leads to greater diffraction and a smaller beam waist. This power loss may affect calculations such as the absorption coefficient by artificially increasing its value. Eq. 4 uses a reference signal to determine the fraction of power absorbed by the sample and calculates the absorption coefficient based on this value and the refractive index. While this equation also takes the thickness of the sample into account, it does not consider the effect it has on the Gaussian Beam coupling. Depending on the material's refractive index and its thickness, the severity of this effect varies.

Theoretically, focal displacement could be accounted for if the optics and receiver could be moved relative to the sample to maximize coupling. If a thick sample were to increase the divergence angle of the beam, the receiver could be moved towards the sample in order to capture the same amount of power that it did in the reference measurement. As previously mentioned, this effect may also be avoided by using thin samples, but sometimes there are advantages to taking measurements with thick materials.

Toptica Systems

Toptica is a Germany based laser manufacturer that produces high end imaging systems. For the purpose of this project, there were two Toptica Systems available for use. The TeraScan which uses continuous wave scanning (CW) and the TeraFlash which uses pulsed imaging. The TeraScan uses GaAs photomixers to produce a continuous THz wave that propagates from an antenna and is then captured by a receiver. The recorded signal may then be processed in a frequency domain analysis shown in Figure 7. CW systems are generally simpler and cheaper than pulsed systems and the frequency domain spectroscopy is easily understood (Karpowicz, 2005). The TeraScan was functional during this project, however an imaging gantry was not yet designed and therefore it was not ready for use.
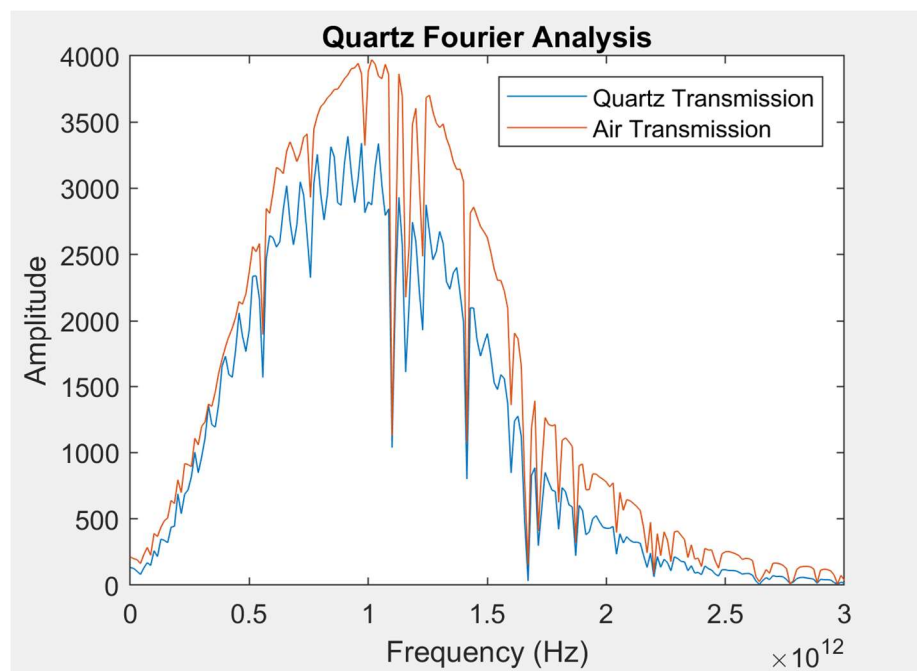
Figure 7. Frequency domain analysis of THz wave through Quartz. The y axis represents the strength of the photocurrent induced by the recorded electromagnetic wave.

The Toptica TeraFlash uses femtosecond lasers to generate THz wave packets that propagate through a sample, then are scanned by the same laser that created them. When data collection begins, a femtosecond laser is fired and split so that half of the laser travels to the

emitter, and half travels towards the receiver. When it reaches the emitter, a DC voltage bias is applied across the photomixer, generating a THz wave packet that is then launched by bowtie antenna. The femtosecond laser that produces the THz pulse is shorter than the wavelength of the THz radiation. Therefore, when the THz wave is received, it must go through a delay stage in which the other half of the split laser scans the wave packet and generates a time domain spectroscopy. An example of this recorded data is shown in Figure 8, and it may then be converted to frequency domain spectroscopy by performing a Fourier analysis, and the power transmitted is proportional to the peak-to-peak Electronic Field. Pulsed systems are generally more complicated than continuous systems, but they can provide more information about a sample. For example, the time difference between a reference and sample signal can be used to determine the optical depth of a known substance. Because we understood how to use the TeraFlash and it was ready for use, it was the main system used in all of the experiments.
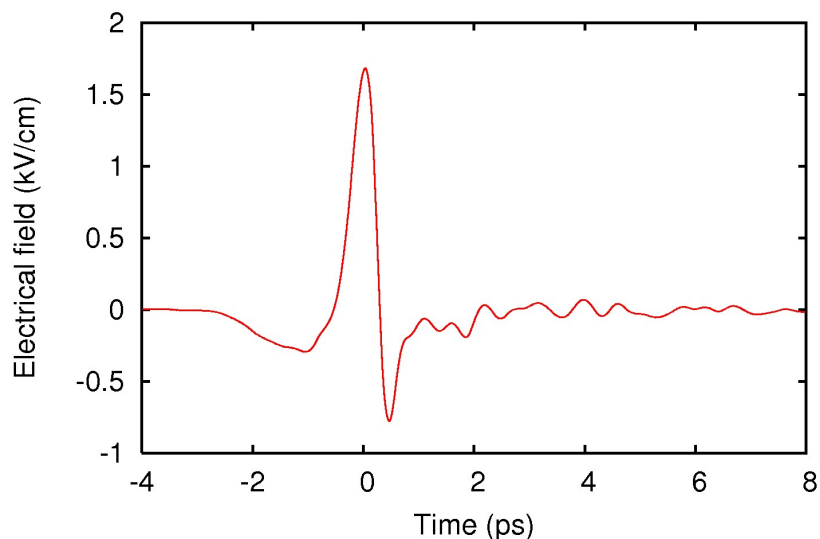
Figure 8. An example of data recorded by time domain spectroscopy. The voltage of the electric field is recorded with respect to time.

While the TeraFlash produces the THz radiation, it does not provide a means of securing or scanning a sample. The Toptica Advanced Terahertz Imaging Platform was used in conjunction with the TeraFlash to take measurements in the THz range. This platform consisted of two linear stage motors that allowed for positioning accuracy of better than 200

µm (Toptica, 2021). This allowed for the use of a focused beam to scan a sample using software provided by Toptica. This system also had a vertical translation stage with a full range of 50 mm that allowed the sample to be moved vertically between the transmitter at the bottom and the receiver at the top. A 3d CAD model of this imaging system may be found in Figure 9. below.
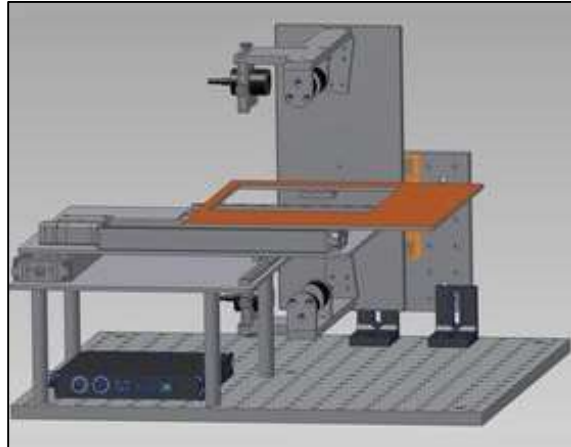
Figure 9. A 3d CAD model of the Toptica Advanced Terahertz Imaging Platform used in conjunction with the Toptica TeraFlash.

The optical components of this imaging gantry are two focusing parabolic mirrors and two collimating mirrors with 1 in diameters. These mirrors are arranged as shown in Figure 10 and are used to both propagate radiation through the system and focus it on the sample. The focal lengths of the focusing mirrors are 4 in and the collimating mirrors have focal lengths of 2 in. This corresponds to a depth of focus of approximately 58.42 µm. This is the length of the focus in which a sample may be placed that provides an acceptable resolution. Figure 10. shows the system to be perfectly coupled, however thick samples will cause focal displacement as seen in Figure 6.
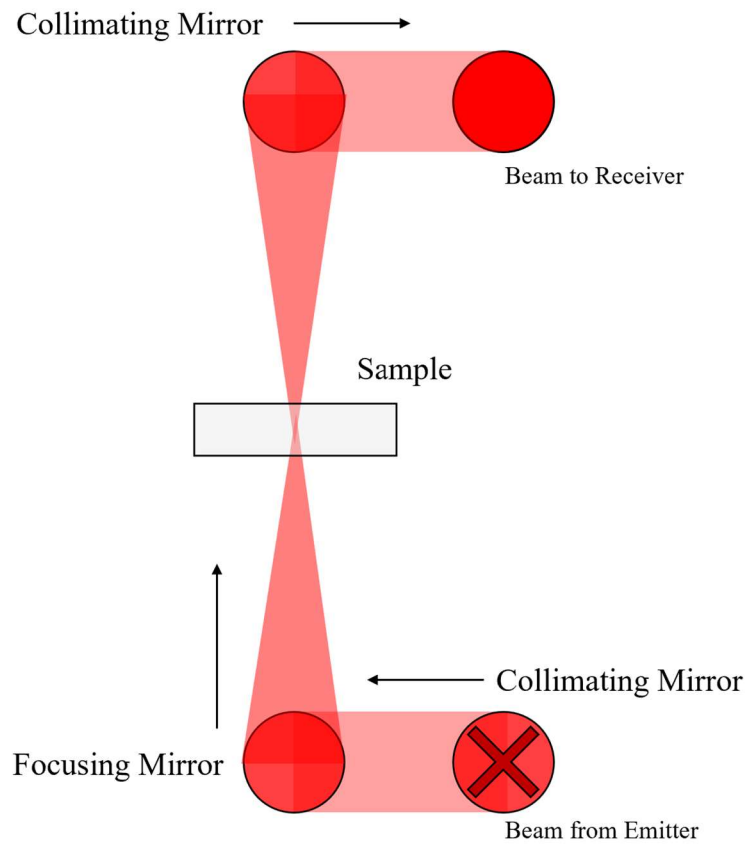
Figure 10. A diagram of how THz radiation is propagated in the Toptica Advanced Terahertz Imaging Platform. The circles denote 90 degree off axis parabolic mirrors, and the shaded red areas are the approximate geometry of the Gaussian Beam.

Experimental Method

TeraFlash Measurements

The first step in using an optical system after setup is to verify whether the system is working properly. There is relatively little knowledge about material properties in the THz spectrum, however some materials such as quartz, fused silica, and Teflon have generally accepted values for refractive index and absorption coefficient based on previous studies (Grischkowsky, 1990). Similar experiments may be repeated and by comparing results, proper use of the TeraFlash can be verified. For the purpose of calculating refractive index and absorption coefficient, a study using time domain THz spectroscopy was repeated. The TeraFlash was used to measure the electric field over time created by the transmittance of THz radiation through samples of 0.7 mm quartz. A Fourier transform was then applied to the collected data to obtain the spectrum transmitted through the sample. From here, Eq. 3 to calculate the refractive index.

The calculated refractive index may be plotted as a function of frequency so its value may be obtained across the THz spectrum. Absorption coefficient is then calculated as a function of frequency with Eq. 4. These equations were translated into MATLAB code that calculated refractive index and absorption coefficient across frequencies from 0.5 to 5 THz. This code may be found in Appendix A and Appendix B. These values were then printed in the form of a graph with the absorption coefficient as a function of frequency, and a table containing all values in the graph. This code may also be used for future calculations using the TeraFlash.

Vertical Scan

When considering the focal displacement in the TeraFlash, it is valuable to first observe the effect of sample position in a focused Gaussian Beam. There is no marked center on the current imaging system, and therefore the center needs to be experimentally determined. An approximate center may be eyeballed; however, this does not maximize the power transmitted at the focus. In order to locate the center of the Gaussian beam, the intensity of the transmitted beam was recorded with respect to time. During data collection, the vertical translation stage was used to move a single slide vertically through the Gaussian

Beam. In doing so, an intensity maximum may be located at approximately the center of the beam which would be ideal for collecting data in order to maximize spatial resolution.

For this experiment, a slide of Fused Silica with a thickness of 0.7 mm was used, and the beam was focused on the center of the slide. Four trials were conducted in which the slide was moved vertically through the beam in 5 mm increments and held at each position for 10 seconds each. In the first trial, the slide began at the center position and was moved upwards towards the receiver to a maximum of 25 mm from its starting position. From here, it was then moved back to its starting position, then down 25 mm towards the emitter. As previously mentioned, the intensity was recorded in arbitrary units every 0.5 seconds and was plotted with respect to time. It should be noted that movement between positions was done at a slow pace in an attempt to improve consistency. Travel occurred over approximately 15 seconds on average leading to a total data recording time of 250 seconds.

For the second trial, the slide started at the lowest point closest to the transmitter, then moved upwards towards the receiver. The same increments of 5 mm for 10 seconds were used for this trial. A third trial was conducted in which the slide began at the point closest to the receiver, then moved downwards towards the emitter in the same increments. These two trials were then averaged together where data from trial 3 was reversed to align with the positions in trial 2. While this alignment was not perfect, the slow adjustments and 10 second period per position allows for a relatively high degree of accuracy.

Slide Stack Measurements

An experiment was then conducted to observe the effects of focal displacement on the TeraFlash' s current system and observe whether it had a significant effect on collected data. For this experiment, a single slide was placed in the imaging gantry and a time domain spectroscopy analysis was conducted. Then, another slide was placed on top of the first and data was collected again. This was repeated once more with a third slide being placed on the stack. Slides of Fused Silica with thicknesses of 0.7 mm each were used for this experiment and the slides were positioned at the approximate center of the focused Gaussian Beam. This experiment was repeated in three separate trials each conducted 20 minutes apart. Given the time domain data, a Fourier Transform was applied, and the refractive index and absorption coefficient were calculated at each of the stack's thicknesses.

Absorption coefficient, α, is a property of a material given in the expression of the Lambert Beer law in Eq. 2. By stacking slides on top of each other, density could be preserved while theoretically increasing the effects of focal displacement and not just due to absorption in the material. It was hypothesized that adding slides would increase the calculated absorption coefficient by a noticeable amount due to increasing divergence angles as a result of focal displacement. To observe this, the absorption coefficient at a frequency of 2 THz was calculated for each trial and averaged together along with the standard deviation. Overall changes in the absorption coefficient as a function of sample thickness could then be analyzed.

Parabolic Mirror Evaluation

Once focal displacement in the imaging system were observed, the next step would be to design an optical system that could adjust for it. Some of the most important components of this system are its focusing elements, specifically its off axis parabolic mirrors. The system was designed for use with the Toptica TeraScan since it was a simpler system that lacked its own imaging gantry. If the system could be shown to account for the effects of focal displacement, it could then be modified and used with the TeraFlash.

The first step in evaluating parabolic mirrors for this system was to determine the *f number* of the parabolic mirror that would capture most of the THz wave emitted. This number was calculated by considering the divergence half angle of the emitted wave, the focal length of the mirror, and the diameter of the mirror. These three values were involved in a trigonometric relationship that could be reduced to the equation below.

$$N = \cot(\theta_{div}) \tag{7}$$

Where N is the *f number*, and θ_{di} is the divergence half angle. A parabolic mirror with this *f number* would maximize the power captured from the emitter. Using this *f number*, the omega at the focal length, or dispersive power, could be calculated for each mirror looked at using the equation below.

$$\omega = \tan(\theta_{div}) * f \tag{8}$$

Where f is the focal length of the parabolic mirror. Using these values, the power collected by the mirror could be calculated by integrating the normal Gaussian Beam power function over the aperture of the lens. This integral may be found below.

$$\frac{P_{aperatur}}{P_0} = \int_0^r e^{\frac{-2x^2}{\omega^2}} dx \tag{9}$$

Where r is the radius of the lens. The fraction of power as defined by the beam radius is also included in his equation. This integral could also be calculated to infinity to calculate the total power of the Gaussian Beam. By then dividing the captured power by the total power, the fractional power captured by each mirror could then be calculated. Next, the new divergence angle of the beam after it was reflected by the mirror was calculated using the Eq. 6. This calculation offered insight as to how the beam would propagate after interacting with the mirror and helped the design of a complete imaging system.

Results

TeraFlash Measurements

The figure below shows the calculated and accepted values of the refractive index of quartz over the bandwidth of 0 to 2 THz. While the TeraFlash is capable of measurements over a bandwidth of over 5 THz, most studies observe the lower range of the THz spectrum. The y axis was initially scaled to match that of the accepted values graph but had to be broadened to capture the general trend of the data.
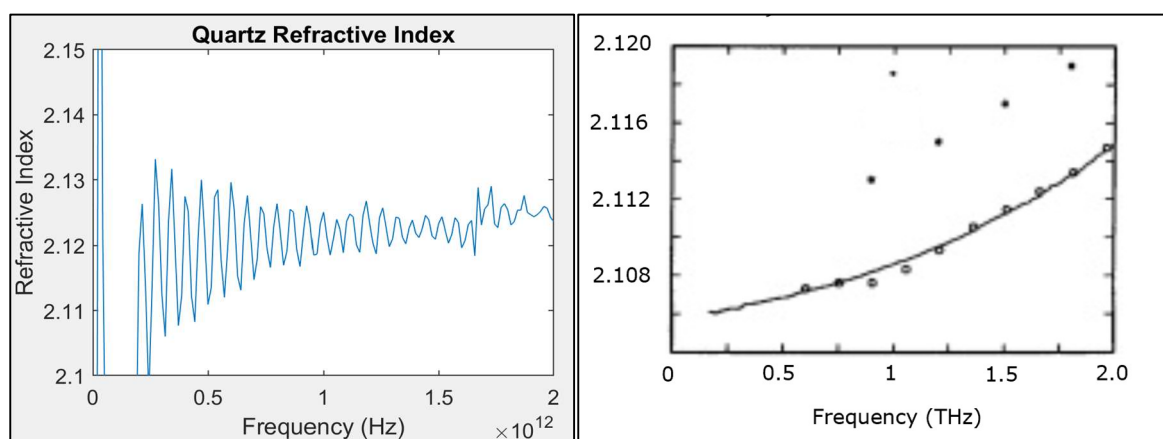
Figure 11. The calculated refractive index of 1 mm thick quartz (left) and accepted the accepted value of the refractive index of quartz from another study (right).

The most immediately obvious characteristics of the calculated refractive index of quartz is the large dip in between 0 THz and 0.25 THz, as well as the oscillations seen throughout the graph. The dip is caused by the TeraFlash' s sensitivity in the low THz range as well as the algorithm's sensitivity to noise. The oscillations are a product of the etalon effect in which radiation reflects off of the inner surfaces of the samples, and smaller pulses of intensity follow the initial transmission signal. With thicker samples, the time in between the initial signal and subsequent pulses is extended to a degree that it may be cleaned out of the data. To observe the accuracy of these calculations, the refractive index may be calculated at a frequency and compared with the accepted value. For the purpose of this analysis, 0.5 THz was used as an indicator of the calculation's accuracy.

The accepted refractive index of quartz at 0.5 THz was found to be approximately 2.106 based on Figure 11. In order to account for the etalon effect, the approximate center of the oscillations at 0.5 THz was taken to be the refractive index. This value was approximately 2.12 indicating an error of 0.014 or 0.66%. For our purposes this is a remarkably low error, indicating that this method for calculating the refractive index in the THz range may be accurately used for other materials.

The calculated absorption coefficient as well as the accepted value of the absorption coefficient for quartz may be found in the figure below. The absorption coefficient was also calculated over a bandwidth of 2 THz and was based off of the refractive index calculations above. Units for both of these graphs are in cm^{-1} even though is not indicated in the accepted values figure.
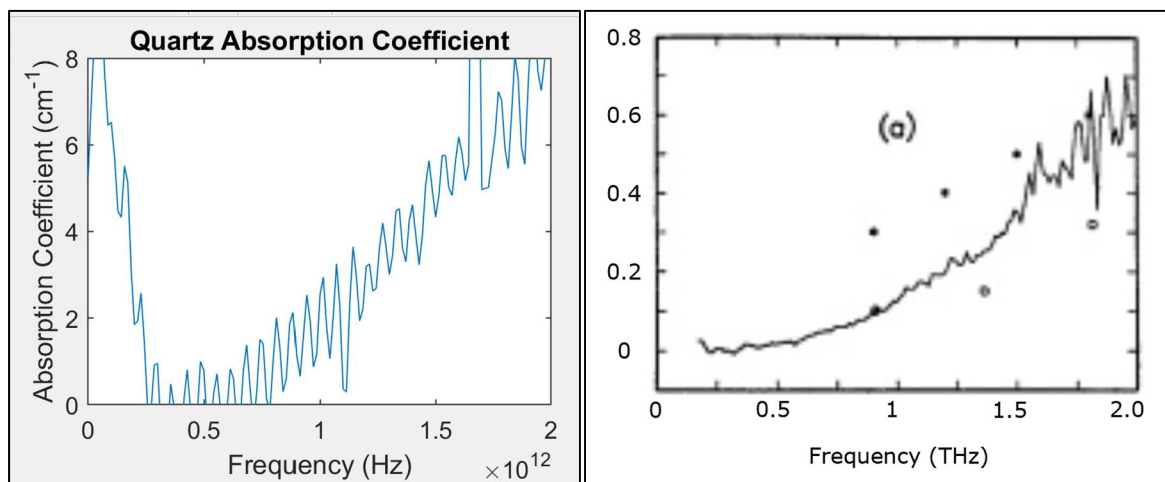
Figure 12. The calculated value of the absorption coefficient of 1 mm quartz (left) as well as the accepted absorption coefficient from a different study (left).

As is expected, the spike at low frequencies and the etalon effect are still prevalent in this data. The general trend of the data in the accepted is also prevalent in the calculated values indicating a degree of accuracy. However, the actual values of the absorption coefficient in the calculated data are approximately 10 times larger than that of the accepted values. Normally, this indicates a minor rounding or units' error, however this may be

debunked when the equation is observed. The inputs to the absorption coefficient equation are the thickness of the sample, the refractive index, the amplitude of the sample signal, and the amplitude of the reference signal. The refractive index was found to be accurate, and the thickness of the sample was used in these calculations, therefore the error must be in the processing of the signal amplitudes. The algorithm is sensitive to noise at low frequencies so this may be the source of the error, however further experiments need to be conducted to verify this. Regardless, the accuracy of the refractive index and the similar trends in calculated and accepted values gives merit to these calculations.

Vertical Scan

The figure below displays the collected intensity vs time for the first trial of the vertical scan experiment. This experiment used one slide of Fused Silica with a thickness of 0.7 mm which began in the middle, traveled up towards the receiver, and then down towards the emitter. The intensity is in arbitrary units and its starting value was approximately 511.5 a.u.
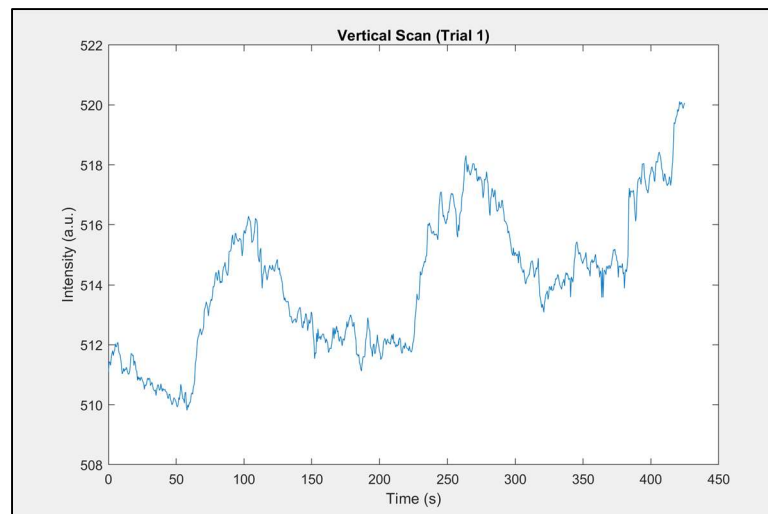
Figure 13. The first trial of the vertical scan of a silicon Slide with a thickness of 1 mm.

As it can bee seen in Figure 13. the intensity starts of fairly steady, then increases at approximately 50 seconds and has its first peak at 100 seconds. At this point in the data

collection, the slide was in the position closest to the receiver at one of the widest points of the focused Gaussian Beam. As the slide was translated back to the center position, its intensity dipped to an average slightly higher than its starting value between 150 and 230 seconds. This is when the slide was moved back to its assumed center before being translated towards the emitter. After the slide passed the midpoint, its intensity increased again and reached a second peak at 250 seconds. At this point, the slide was 15 mm away from the emitter. When the slide reached the position closest to the emitter at 300 seconds, the intensity dropped to a value slightly higher than the previous measurement at the assumed center. Then, as the slide was translated back towards this center, it increased towards its highest peak at the end of data collection. At this point, the slide was stationary at the center and the intensity was measured to be 520 a.u.

This data revealed an inconsistent relationship between slide position and overall intensity. The first two times the slide was in the center position, it had its lowest relative intensity measurements, but the third time it was centered, it peaked. Additionally, this trial indicated that more power was transmitted at a position closest to the receiver, and 15 mm away from the transmitter. This does not reflect the expected measurements of a symmetric, focused Gaussian Beam. However, there was also only a variation of about 10 a.u. or 1.9% from the intensity's lowest value which could be attributed to system drift.

The next two trials were conducted as a pair in an attempt to remove the effects of system drift on the calculations. The maximum intensity at the center of the beam was expected to be relatively small, and therefore it would be easily disguised by noise or system drift. To try to accommodate for this, the second trial only moved the slide upwards over a period of 250 seconds, and the third trial moved it downwards. It can be seen from the data that there was a noticeable increase in starting intensity between trials two and three which were conducted 20 min apart. This is a result of natural system drift in which the TeraFlash' s measurements become more consistent the longer that it is running.
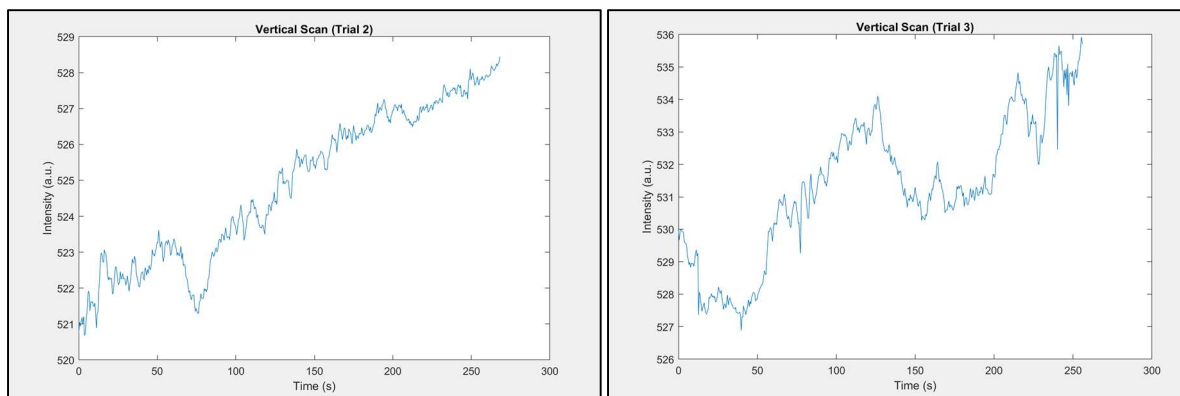
Figure 14. The second and third trial results from the vertical scan.

An upward trend in intensity is immediately evident in trials two and three which is also likely an artifact of system drift. Based on these datasets there is no immediately clear position at which the maximum intensity would be transmitted through the sample. Further processing of this data is shown below in figure 15.
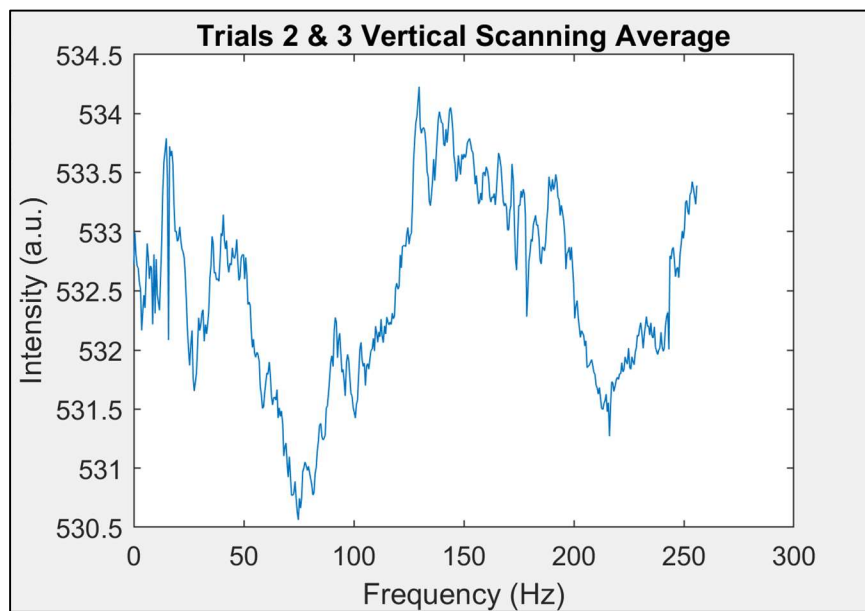
Figure 15. This figure shows the average of trials two and 3 in which the data was arranged so that the time in each data set corresponded to approximately the same position.

This graph is the average of the intensities over time of trials two and three. There was some manipulation of both data sets, however, so that they could be properly averaged together. First, the intensity measurements of trial 2 were translated up by 9 a.u. so that both sets would have the same starting point. Because intensity is measured in a.u. this does not have a significant impact on the accuracy of the measurement. Additionally, the important factor of this data set is not the value of the intensity, but rather its relative magnitude compared to other points within the Gaussian Beam. Next, the data from trial 3 was flipped about the center data point. The scans in trials two and three were conducted in opposite directions, and the intensity values of one of the trials needed to be flipped so that the times along the x axis corresponded to approximately the same position in the beam. It should be noted that the times did not perfectly align between trials due to variations in translation speed, but the 10 second stationary period at each position allowed for comparable data approximately every 25 seconds. In calculating this average, the gradual system increase in intensity over time was averaged out of the original data to provide a more accurate understanding of the relationship between intensity and position.

After trials two and three were averaged, a noticeable peak appeared at approximately 150 seconds with minimums on either side. This region is at the assumed center of the system, and the minimums indicate positions closer to the emitter and receiver. Because trial three was flipped, early points in the data correspond to positions close to the receiver, and later points indicate positions close to the emitter. There are also peaks at the positions closest to the emitter and receiver that occur over a shorter period. While this does suggest that the assumption of maximum transmission at the focal point is true, the peak does not vary by a large amount from the minimum. The difference between the minimum at 75 seconds and the maximum at 150 seconds is approximately 4 a.u. or 0.75%. Such a small variation may still be a product of system drift, but if more trials with different materials yielded similar results, our hypothesis may be comfortably supported. Additionally, if the motion of the sample in the Gaussian Beam was motorized, this would lead to a more consistent relationship between position and signal amplitude.

Slide Stack Measurements

Figure 16. shows an example of the calculated absorption coefficient for a stack of three Fused Silica slides. The etalon effect was still present in all of these calculations and therefore needed to be accounted for when calculating the absorption coefficient at 2 THz. To do so, the center of an oscillation before 2 THz was selected, and two full oscillations were averaged after this point. This allowed for the average absorption coefficient at 2 THz to be precisely calculated.

Table 1. (left) The average absorption coefficients for different thicknesses of Fused Silica samples

Sample Thickness (cm)	Absorption Coefficient (cm⁻¹)
0.07	9.12 ± 0.99
0.14	12.13 ± 0.31
0.21	12.54 ± 0.28
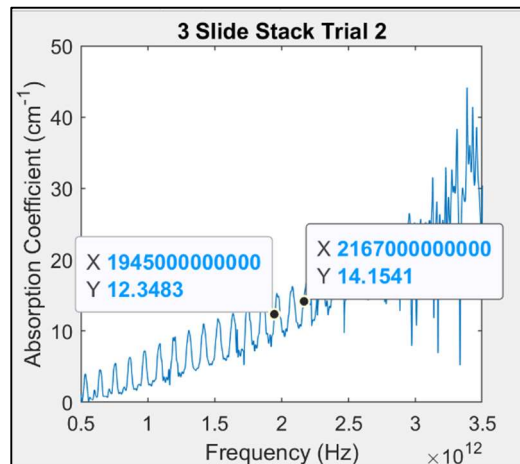
Figure 16. (right) An example of the region used to calculate absorption coefficient.

While the first experiment indicated that the absorption coefficient could not be calculated accurately, repeated trials revealed precision in these calculations. In this way, the change in absorption coefficient with respect to sample thickness could be determined through this experiment. As shown in Table 1. there was an increase in the absorption coefficient of approximately 33% between thicknesses of 0.07 and 0.14 cm. As previously stated, absorption coefficient is not dependent on thickness, and therefore this is likely a product of focal displacement. There was less of an increase between 0.14 and 0.21 cm at approximately 3.4% which does not indicate significant focal displacement influence. The

results of this experiment support our hypothesis that focal displacement is a significant source of error in the current TeraFlash imaging system.

Parabolic Mirror Evaluation

In total, 18 different parabolic mirrors were evaluated from four different companies, all with bare gold lenses. For practicality, the target mirror diameter was 2 in. and the calculated target $f/\#$ was 4.48 based on the TeraScan divergence angle of 7 degrees at 500 GHz. While the system would be used with frequencies that were much greater, 500 GHz was the highest frequency at which the TeraScan's divergence angle was experimentally determined (Kolpatzek, 2019). For the full excel table of evaluated parabolic mirrors, see Appendix C.

Table 2. below shows the characteristics of four different parabolic mirrors from ThorLabs (ThorLabs, 2021). The mirrors' focal lengths ranged form 2 in to 6 in and the mirror with the closest f/# to the desired value had an $f/\#$ of 3.00. This mirror also had a fractional power of 0.864 and would result in a new divergence angle of 0.215 degrees. This makes this mirror an excellent option for the new optical system, especially considering ThorLabs' strong reputation for manufacturing optical equipment. In the following tables, $f/\#$ was calculated using Eq. 7, Omega at focal length was calculated using Eq. 8, captured power was calculated using Eq. 9, and the new divergence angle was calculated using Eq. 6.

Table 2. Off axis parabolic mirror evaluation for four ThorLabs mirrors.

Company	Price	Diameter (in)	Reflected Focal Length (in)	Parent Focal Length (in)	f/#	Omega @ Focal Length	Captured Power	Total Power	Fractional Power	New Divergence Angle (Degrees)
ThorLabs	$353.86	2	2.000	1.000	1.00	0.208	0.113	0.130	0.865	0.215
			3.000	1.500	1.50	0.312	0.169	0.195	0.865	
			4.000	2.000	2.00	0.416	0.225	0.260	0.865	
			6.000	3.000	3.00	0.623	0.337	0.391	0.864	

The next company whose mirrors were evaluated was Newport Photonics, another company with a strong reputation for quality optics components. Unfortunately, Newport did not sell mirrors with diameters of 2 in, only mirrors with diameters of 1.5 in and 3 in

(Newport Photonics, 2021). With that said, Newport's mirror with a focal length of 8.000 had an f/# of 5.33 which is only about 18.9% different from our target f/#. However, due to the smaller diameter of the mirror, the fractional power is 0.851: a 0.013 difference from the ThorLabs mirror. The new divergence angle is also slightly larger at 0.287 degrees.

Table 3. The characteristics of four parabolic mirrors from Newport Photonics.

Company	Price	Diameter (in)	Reflected Focal Length (in)	Parent Focal Length (in)	f/#	Omega @ Focal Length	Captured Power	Total Power	Fractional Power	New Divergence Angle (Degrees)
Newport	$345.00	1.5	2.000	N/A	1.33	0.208	0.113	0.130	0.865	0.287
			4.000	N/A	2.66	0.416	0.225	0.260	0.865	
			6.000	N/A	4.00	0.623	0.337	0.391	0.864	
			8.000	N/A	5.33	0.831	0.443	0.521	0.851	

Next, four mirrors from Highlight optics were characterized with focal distances ranging from 2 in to 10 in (Highlight Optics, 2021). Highlight Optics is a relatively new and unknown company, and therefore we are uncertain of the quality of their lenses. The mirror with the focal length of 10 in had an f/# of 5.00 which was 0.52 away from our target value. When calculating the fractional power however, the larger focal distance led to a power loss 0.056 greater than ThorLabs' mirror. These mirrors also had the same new divergence angle as the ThorLabs mirrors.

Table 4. The characteristics of four off axis parabolic mirrors from Highlight Optics.

Company	Price	Diameter (in)	Reflected Focal Length (in)	Parent Focal Length (in)	f/#	Omega @ Focal Length	Captured Power	Total Power	Fractional Power	New Divergence Angle (Degrees)
Highlight Optics	$340.00	2	2.000	N/A	1.00	0.208	0.113	0.130	0.865	0.215
			4.000	N/A	2.00	0.416	0.225	0.260	0.865	
			6.000	N/A	3.00	0.623	0.337	0.391	0.864	
			10.000	N/A	5.00	1.039	0.533	0.651	0.818	

The last series of mirrors that were evaluated were six mirrors from Edmund Optics with focal lengths ranging from 2.000 in to 7.500 in (Edmund Optics, 2021). Edmund Optics

is another well known optics company that manufactures components for systems in the THz range. The mirror with the closest f/# to our target value was the mirror with 7.500 in focal length and an f/# of 3.75. This mirror was similar to the previously mentioned mirror from Highlight Optics in that its long focal length resulted in a lower fractional power captured. This mirror captures 0.856 of the total power, a 0.008 decrease from the ThorLabs mirror. This is a relatively small difference, especially compared to the Highlight Optics mirror.

Table 5. The characteristics of six off axis parabolic mirrors from Edmund Optics.

Company	Price	Diameter (in)	Reflected Focal Length (in)	Parent Focal Length (in)	f /#	Omega @ Focal Length	Captured Power	Total Power	Fractional Power	New Divergence Angle (Degrees)
Edmund Optics	$408.00	2	2.000	1.000	1.00	0.208	0.113	0.130	0.865	0.215
			3.000	1.500	1.50	0.312	0.169	0.195	0.865	
			4.000	2.000	2.00	0.416	0.225	0.260	0.865	
			6.000	3.000	3.00	0.623	0.337	0.391	0.864	
			7.000	3.500	3.50	0.727	0.392	0.456	0.860	
			7.500	3.750	3.75	0.779	0.418	0.488	0.856	

After reviewing each of the mirrors, the Thorlabs parabolic mirror with an f/# of 3.00 was determined to be the best option. This mirror collected a large fractional power compared to mirrors of similar size. The Newport Photonics mirror also captured a high fractional power, but its smaller size was not what the system was initially designed for. The Edmund Optics also had a relatively high captured power, but it was noticeably more expensive than the ThorLabs mirror. The ThorLabs parabolic mirror captured a high fraction of power for an affordable price from a reputable company. Given these factors, it was chosen as the mirror to be implemented in the new optical system.

Conclusion

This project verified a method for accurately calculating refractive index using the TeraFlash, identified focal displacement as a source of error in these measurements, and started the design of an optical system that could circumvent this error. The fundamental Gaussian Mode was found to be an effective method for modeling THz radiation for imaging purposes. Using this model, eq 1. may be used to accurately calculate the refractive index despite oscillations created by the etalon effect. In the future, thick samples may be used to separate secondary pulses from the primary transmission and smooth the data. By using this method to calculated refractive index, materials can be characterized for use in THz optical systems. Accurate values were not calculated for the absorption coefficient, but accurate trends were created using Eq. 2. The values in these calculations were greater than accepted values by a factor of 10 and were impacted by the etalon effect. The source of error in these calculations was identified to be in either the way the signal amplitude was processed or the raw signal itself. This experiment may be replicated with other well-known materials to observe how consistent this phenomenon is. A software other than MATLAB could also be used for the same purpose to check whether there was an unknown error in the way the operations were performed. By refining these methods for calculating refractive index and absorption coefficient, materials of unknown qualities may be characterized for use in THz systems.

The vertical scan experiment yielded some indication of a maximum power transition when the sample is centered at the focal point. This maximum was not significant though, and further iterations need to be performed with different materials to observe whether this behavior is consistent. In doing so, a method for locating the center of the Gaussian Beam may be developed so that the spatial resolution of focused beam scan can be maximized. For the time being, it is sufficient to assume the center of the Gaussian Beam to be at the center of the translational stage. Because the maximum cannot be easily determined by the vertical scan experiment, an off-center sample is unlikely to significantly affect the quality of collected data.

Focal displacement was found to be a significant source of error in the current TeraFlash imaging system. While this is not present in the measurements of thin films, there

is a need to image thick samples. Thick samples can be used to remove the etalon effect when calculating absorption coefficient, creating smoother data sets. Additionally, optical lenses often reach thicknesses that would induce the focal displacement effect which restricts our ability to understand lens properties. Therefore, the next step is to develop an imaging system that account for focal displacement by adjusting the receiver position with respect to the sample. The system would then be able to scan the receiver through its different positions and identify a location that maximizes transmission. At this location, the absorption coefficient should be measured to be the same as with thin samples.

When designing this system, it was determined that 2 in diameter, 3.00 f/# off axis parabolic mirrors from ThorLabs were the ideal lenses. These mirrors provided a high fraction of captured power and a small new divergence angle after the beam interacts with the lens. These mirrors provide the mechanics for propagating light throughout the imaging system, but structural components need to be implemented as well. Below is a prototype for an imaging gantry that would allow for both horizontal and vertical scanning of a sample using the TeraFlash or TeraScan system. It consists of linear and vertical stages manufactured by Zaber, and structural components consisted of ThorLabs breadboards. This model does need refinements, but it may be used as the basis to develop a system that can account for the previously measured errors and accurately determine optical properties of materials in the THz range.
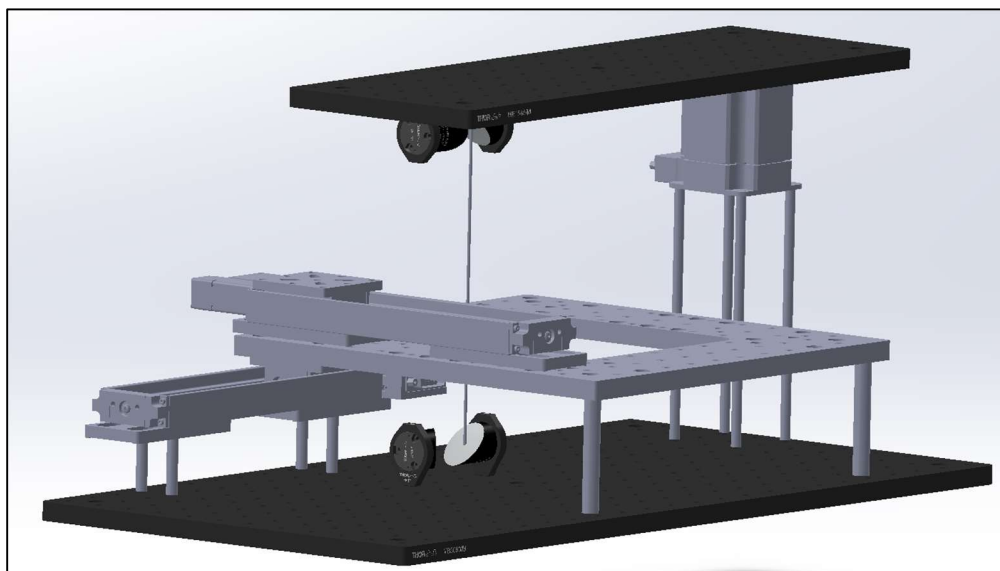
Figure 17. 3d CAD model of an imaging gantry that can horizontally and vertically scan.

References

Chong Han, Yongzhi Wu, Zhi Chen, & Xudong Wang. (2019). Terahertz

    Communications (TeraCom): Challenges and Impact on 6G Wireless Systems.

Edmund Optics. (2021). *Gold Off-Axis Parabolic Mirrors: Edmund Optics. Edmund Optics*

    Worldwide. https://www.edmundoptics.com/f/gold-off-axis-parabolic-mirrors/39489/.

Felix Abt, A. H. and F. D. (2008, May 1). Focusing High-Power, Single-Mode

    Laser Beams. Photonics Media. https://www.photonics.com/Articles/Focusing_High-
    Power_Single-Mode_Laser_Beams/a33535.

Grischkowsky, D., Keiding, S., van Exter, M. and Fattinger, C. (1990).

    "Far-infrared time-domain spectroscopy with terahertz beams of dielectrics and
    semiconductors," J. Opt. Soc. Am. B 7, 2006-2015

Highlight Optics. (2021). OAP, Off-axis Parabolic Mirrors, Protected Gold coating OAP,

    Protected Silver OAP. http://www.highlightoptics.com/en/Product/340.html.

Karpowicz, N., Zhuong, H., Xu, J., Lin, K., Hwang, J. and Zhang, X. (2005). Comparison

    between pulsed terahertz time-domain imaging and continuous wave terahertz
    imaging. *Semiconductor Science and Technology.* (20). DOI:
    https://doi.org/10.1088/0268-1242/20/7/021

Kolpatzeck, K., Liu, X., Friederich, B., Damyanov, D., Häring, L., Schultze, T., Balzer, J., &

    Czylwik, A. (2019). Wideband Radiation Pattern Measurement of Terahertz Antenna-
    Integrated Photodiodes by Frequency-Domain Spectroscopy. In 2019 Second
    International Workshop on Mobile Terahertz Systems (IWMTS) (pp. 1-5).

Liang, Q., Klatt, G., Krauß, N., Kukharenko, O., & Dekorsy, T. (2015). Origin of potential

    errors in the quantitative determination of terahertz optical properties in time-domain
    terahertz spectroscopy. Chinese Optics Letters, 13, 093001-93005.

Murphy, J.A., McCabe, M. & Withington, S. (1997). Gaussian beam mode analysis of the

coupling of power between horn antennas. *Int J Infrared Milli Waves* (18), 501–518. https://doi.org/10.1007/BF02677936

Newport Photonics. (2021). *Off-Axis Replicated Parabolic Mirrors. Off-Axis Parabolic Mirror.* https://www.newport.com/f/off-axis-replicated-parabolic-mirrors.

Paschotta, D. R. (2021, March 10). Beam Divergence. RP Photonics Encyclopedia – beam divergence. https://www.rp-photonics.com/beam_divergence.html.

ThorLabs. (2021). *Off-Axis Parabolic Mirrors, Unprotected Gold Coating.* https://www.thorlabs.com/newgrouppage9.cfm?objectgroup_id=12395.

TOPTICA News. TOPTICA Photonics AG. (2021, February 10). https://www.toptica.com/toptica-news/fast-and-flexible-toptica-presents-advanced-terahertz-imaging-platform/.

Toptica. *Products*. TOPTICA Photonics AG. (2021, April 26). https://www.toptica.com/products/.

Yunshu, G., Chen, X., Chen, G., Tan, Z., Chen, Q., Dai, D., Zhang, Q., & Yu, C. (2019). Programmable Spectral Filter in C-Band Based on Digital Micromirror Device. Micromachines, 10, 163.

Zhang, J., Xia, T., Chen, Q. et al. (2018). Measurement of Absorption Coefficient of Paraformaldehyde and Metaldehyde with Terahertz Spectroscopy. J Appl Spectrosc (85), 84–89. Retrieved from: https://doi.org/10.1007/s10812-018-0616-6

Appendix A

MATLAB code for performing a Fourier analysis on time domain spectroscopy data

```matlab
function [table] = FourierAnalysis(samp, ref, sheetName)

    %Conduct Fourier Analysis and calculate frequencies
    fourier = abs(fft(samp));
    reference = abs(fft(ref));
    fs = 4001/(200*10^(-12));
    frequency = [0:fs/4001:fs-fs/4001].';

    %Calculate phase
    SPhase = angle(fft(samp));
    RPhase = angle(fft(ref));

    %Unwrap phase
    %SPhase = UnwrapPhase(SPhase);
    RPhase = UnwrapPhase(RPhase);

    %Create table with data
    %data = [frequency, fourier, SPhase, reference, RPhase];
    %table = array2table(data);
    %table.Properties.VariableNames = {'Frequency (Hz)', 'Sample', 'Sample Phase', 'Reference', 'Reference Phase'};

    %export table
    writetable(table, sheetName);

    %plot fourier analysis
    %plot(frequency, fourier);
    %hold on
    %plot(frequency, reference)
    %hold off
    %xlim([0 3*10^12])
    plot(frequency,SPhase)


end

function [UnwrPhase] = UnwrapPhase(phase)

    threshold = pi;
    N = 1401;
    for i = 1:N-1
        if(phase(i+1) - phase(i) > threshold)
            for j = i+1:N
                phase(j) = phase(j) - 2*pi;
            end
        else
            if(phase(i+1) - phase(i) < -threshold)
                for j = i+1:N
                    phase(j) = phase(j) + 2*pi;
                end
            end
        end
    end

    UnwrPhase = phase;
end
```

Appendix B

MATLAB code for calculating refractive index and absorption coefficient

```matlab
function [] = AbsorptionCoefficient(Aref,Asam,P,f,d,absTableName,refracTableName)
    Aref = Aref(2:end);
    Asam = Asam(2:end);
    P = P(2:end);
    f = f(2:end);
    coeffs = absCoeff(Aref,Asam,P,f,d);
    %absorption = mean(rmmissing(coeffs));
    coeffs = smooth(coeffs);
    figure(1)
    plot(f,coeffs)
    xlim([0.5*10^12 3.5*10^12])

    n = refInd(P,f,d);
    figure(2)
    plot(f,n)
    xlim([.5*10^12 3.5*10^12])

    tables(f,coeffs,n,absTableName,refracTableName);
end

function [n] = refInd(P,f,d)
    n = 1 + (P*3*10^10)./(2*pi*f*d);
end

function [absCoeff] = absCoeff(Aref,Asam,P,f,d)

    n = refInd(P,f,d);
    plot(f,n)
    absCoeff = (2/d)*log((Aref./Asam).*((4*n)./((n+1).^2)));

end

function [] = tables(f,coeffs,n,absName,refracName)
    abs = [f, coeffs];
    refrac = [f, n];
    abstable = array2table(abs);
    refractable = array2table(refrac);
    abstable.Properties.VariableNames = {'Frequency', 'Absorption Coefficient'};
    refractable.Properties.VariableNames = {'Frequency', 'Refractive Index'};

    %Write Tables
    writetable(abstable,absName);
    writetable(refractable,refracName);

end
```

Appendix C

Parabolic mirror evaluation table

Company	Mirror	Price	Diameter (in)	Reflected Focal Length (in)	Parent Focal Length (in)	f Number	Omega @ Focal Length	Captured Power	Total Power	Fractional Power	New Divergence Angle (RAD)	New Divergence Angle (Degrees)
ThorLabs	MPD229	$ 353.86	2	2.000	1.000	1.000	0.208	0.113	0.130	0.865	0.004	0.215
	MPD239			3.000	1.500	1.500	0.312	0.169	0.195	0.865		
	MPD249			4.000	2.000	2.000	0.416	0.225	0.260	0.865		
	MPD269			6.000	3.000	3.000	0.623	0.337	0.391	0.864		
Edmund Optics		$ 408.00	2	2.000	1.000	1.000	0.208	0.113	0.130	0.865	0.004	0.215
				3.000	1.500	1.500	0.312	0.169	0.195	0.865		
				4.000	2.000	2.000	0.416	0.225	0.260	0.865		
				6.000	3.000	3.000	0.623	0.337	0.391	0.864		
				7.000	3.500	3.500	0.727	0.392	0.456	0.860		
				7.500	3.750	3.750	0.779	0.418	0.488	0.856		
Newport	50329AU	$ 345.00	1.5	2.000	N/A	1.333	0.208	0.113	0.130	0.865	0.005	0.287
	50338AU			4.000	N/A	2.667	0.416	0.225	0.260	0.865		
	50331AU			6.000	N/A	4.000	0.623	0.337	0.391	0.864		
	50332AU			8.000	N/A	5.333	0.831	0.443	0.521	0.851		
Highlight Optics	OAP-2202*	$ 340.00	2	2.000	N/A	1.000	0.208	0.113	0.130	0.865	0.004	0.215
	OAP-2402			4.000	N/A	2.000	0.416	0.225	0.260	0.865		
	OAP-2602*			6.000	N/A	3.000	0.623	0.337	0.391	0.864		
	OAP-21001**			10.000	N/A	5.000	1.039	0.533	0.651	0.818		